JTTEE5 9:73-82




# Characterization of Copper Layers Produced by Cold Gas-Dynamic Spraying

*R.C. McCune, W.T. Donlon, O.O. Popoola, and E.L. Cartwright*

*(Submitted 26 January 1999; in revised form 6 December 1999)*

**The cold gas-dynamic spray method produces coatings or deposits by introducing solid feedstock particles into a supersonic gas stream developed through the use of a converging-diverging (de Laval) nozzle. The particles thus accelerated impact on a substrate surface and develop into a dense deposit through a process believed to be similar to cold compaction. The work reported here explores the internal nature and physical characteristics of copper deposits produced by the cold gas-dynamic spray method using two vastly different starting powders: in one case, a "spongy" copper obtained by a direct-reduction process, and in the second, a denser, more spheroidal particulate produced by gas atomization. Optical and electron microscopies (scanning electron microscopy [SEM] and transmission electron microscopy [TEM]) were used to observe details of microstructure in the feedstock particles and deposits. Young's modulus and residual stress measurements for the deposits were obtained through mechanical means, and measurements of hardness and electrical conductivity are reported. The internal structure of the cold-spray deposit was influenced by the surface purity of the feedstock material.**

**Keywords** cold spray, impact fusion, copper

## 1. Introduction

In the majority of practical applications of thermal-spray technology, the spray process is characterized by a liquefaction step of feedstock material in the form of powder or wire, followed by projection of the droplets so generated onto a substrate where rapid solidification and material buildup occur. One contribution to the intrinsic residual stress state in thermal-spray coatings results from the quenching stress accompanying the rapid solidification and cooling process of droplets coalescing on the developing layer.[1] Additionally, the thermal energy required for producing molten feedstock droplets generally through use of flames, plasmas, or arcs causes some degree of oxidation in most metals used to develop thermal-spray coatings and in thermal degradation or sublimation of compounds such as metal carbides. Oxidation of the coating may be reduced or eliminated through use of vacuum or inert gas-filled chambers or by inert gas shrouding.

Production of coatings with favorable states of residual stress have been obtained previously through use of detonation guns[2] or HVOF (high-velocity oxy-fuel) torches,[3] which achieve conditions where the state of the particles at impact may be semi-solid. A mapping of the pressure/temperature regimes for high-velocity, oxyfuel deposition was proposed by Browning,[4] where the microstructure of the developing coating was related to the physical state of particles on impact. The region of equiaxed, nonliquid particle coalescence was defined as "impact fusion" to distinguish it from coating formation obtained from more liquidlike particles. A methodology for production of surface coatings of limited thickness on the order of several micrometers, from metallic particles in solid form, was shown by Rocheville.[5] The process employed a supersonic nozzle into which solid particles of the feedstock material were introduced and accelerated toward a substrate, where they impinged to produce thin surface coatings, or were directly embedded as isolated particles in small depressions on the substrate surface.

The development of a method for producing thick deposits of various metals from "cold" jets was reported by Alkhimov *et al.* in 1990,[6] and later in a U.S. Patent.[7] In this particular approach to impact fusion, solid particles in the preferable size range of 10 to 50 $\mu$m are introduced by means of a pressurized powder feeder into the high-pressure, high-temperature chamber of a converging-diverging (de Laval) nozzle and are accelerated into a supersonic stream by the propellant gas, which has been electrically preheated prior to introduction into the nozzle. There is no combustion process or electrical discharge in the spray device itself. A unique attribute of cold gas-dynamic spraying is its ability to generate a wide range of deposited layer thicknesses ranging from tens of microns up to as much as a centimeter. In this regard, the process extends beyond the concept of "coating" of a substrate and includes the capability of developing three-dimensional structures. In a recent development, Gabel and Tapphorn[8] reported a spray forming process using a low-temperature gas stream and solid particle introduction into an accelerating jet. Bhagat *et al.*[9] reported the use of the cold spray process for production of nickel-bronze layers used for wear resistance. The work presented here follows several earlier, more general reports on cold gas-dynamic spraying conducted as part of a consortium program.[10,11,12] This work focuses on the microstructural and physical characteristics of copper deposits made by cold gas-dynamic spraying using two morphologically different copper powders as feedstock materials. Microscopic characteristics of both the starting powders and deposits were examined to gain understanding of the nature of particle-to-particle bonding, which occurs in the compact, and moreover to assess the nature of deformation and recovery associated with the deposit formation process.

**R.C. McCune, W.T. Donlon, O.O. Popoola,** and **E.L. Cartwright,** Ford Motor Company, Dearborn, MI 48121.

## 2. Theoretical Aspects

While a complete formalism for the process of coating development in cold gas-dynamic spraying has not fully emerged, Dykhuisen and Smith[13] have developed a model for particle kinetics associated with cold-spray nozzles. The coating development process is believed to be analogous to explosive or impact compaction, wherein localized pressure waves develop in the solid state upon impact of the incoming particles producing deformation both in the impacting particle and the substrate. Studies of impact compaction of stainless steel particles have been conducted by Raybould.[14] In cold gas-dynamic spraying, the kinetic energy of the incoming particles is converted, in part, to localized heating as well as plastic deformation of both substrate and particles. Raybould's work[14] illustrated microscopically the occurrence of localized melting at particle junctions occurring at the highest rates of compaction. In Raybould's study, zones associated with interparticle melting could be observed by optical microscopy and were distinguishable from the internal, cold-worked regions of the compacted particles. The liquidlike boundaries were believed to facilitate the compaction process by acting as an interparticle lubricant, as well as readily flowing into interstitial void spaces. One indication of this particular mode of interparticle bonding would, therefore, be the appearance of such melt/solidification zones between particles. Such areas should be distinguishable from the heavily cold-worked particle interiors.

The quality of interparticle bonding in "cold-spray" compacts is expected to be characterized, in part, by the relative ease with which equilibrium grain structures develop *via* coalescence and migration of boundaries formed as a consequence of the cold compaction of the feedstock particles. Internal (*i.e.,* intraparticle) grain boundaries formed upon solidification of the gas atomized powder or by coalescence of particles during the direct reduction process are believed to be capable of ready migration on high-temperature annealing. If the interparticle boundaries are, in some way, pinned by surface oxides or other debris of the deposition process, such a structure could not be rendered into an equiaxed or equilibrium by simple thermal annealing analagous to the sintering of a green powder compact. Annealing studies of cold-sprayed compacts may give some indication of the quality of interparticle boundaries and their ability to relax into more equilibrium-like microstructures.

## 3. Experimental Procedures

### 3.1 Materials

Two widely different feedstock powders were used in this investigation. The intrinsic differences in starting materials are believed to be largely responsible for the nature and properties of the layers subsequently formed by cold spraying. Characteristics of these feedstock powders are summarized in Table 1. The first material studied was a copper powder produced by a direct reduction process, designated SCM- 500RL (SCM Metal Products, Inc., Research Triangle Park, NC). Typical particles of this material are shown in the scanning electron microscopy (SEM) micrograph of Fig. 1. The majority of these particles show highly convoluted surfaces believed to be characteristic of the manner in which the powders are generated. The higher observed oxygen content of the direct-reduction powder is consistent with its greater surface area per unit of mass and ultimately contributes to the trapping of minute oxide particles in the final deposit. A second material studied was designated Acupowder 500 and was produced by inert gas atomization (ACuPowder International, LLC, Union, NJ). Powder particles of this material were characterized by (a) generally dense surfaces (illustrated by Fig. 2), (b) lower oxygen content than direct-reduction powder, and (c) general lack of occluded oxide particles in the deposits formed by cold spraying. Substrates for development of the cold-spray deposits were nominally 3 mm thick (0.125 in.) pieces of commercial, tough-pitch copper (Copper Association designation C11100) which were roughened by grit blasting with alumina powder prior to development of the cold-spray deposits.

### 3.2 Cold Gas-Dynamic Spray Method

Details of the spray process have been previously reported elsewhere.[10,11] Schematization of the spray method and the particular geometry used for the generation of the coupons studied here are illustrated in Fig. 3 and 4, respectively. Operational characteristics of the spray nozzle are included in Table 1. Sprayed layers were generally developed to a thickness of >3 mm, so that specimens for transmission electron microscopy (TEM) could be obtained from sections cut perpendicular to the plane of the substrate, as illustrated in Fig. 4, and so that thick bilayer specimens could be produced for both determination of residual stress and Young's modulus by mechanical means. Specimen strips for these latter determinations involved generation of coupons of approximate size $2.54 \times 15.24$ cm.

### 3.3 Analysis

**Microscopy.** Details of the microstructure of feedstock materials and compacts produced by cold gas-dynamic spraying were determined by optical and electron microscopy. Optical microscopy of the internal structure of feedstock powders was conducted on the gas-atomized Acupowder 500 material by embedding a sample of the powder in an epoxy mount, then polishing and etching with beta-copper etch (30 ml ammonium hydroxide [30% reagent grade], 12 ml hydrogen peroxide [3% solution], and 30 ml distilled water) to reveal details of internal grain boundaries. Powder specimens of the SCM direct reduction copper were mounted similarly although not etched after polishing, since the high degree of internal porosity in these particulates was not amenable to use of the etchant. Similar optical microscopy was conducted on sections of both sprayed compacts to reveal both interparticle and internal boundaries. Scanning electron microscopy was conducted on feedstock particles and on fracture surfaces produced by bending notched millimeter thick pieces of the compact until fracture occurred. Transmission electron microscopy of feedstock powders was conducted on specimens prepared by mounting of particles in a polymeric media, sectioning to produce a disk of diameter 3 mm with thickness of 85 $\mu$m, and dimpling with both diamond and alumina media to a disk thickness of 10 to 15 micrometers. Final ion thinning was conducted by Gatan, Inc. (Pleasanton, CA) using their precision ion polishing system (PIPS) at low angles using 5 keV argon ions. Specimens of the sprayed layers were prepared for TEM by mechanically thinning sections, as illustrated in Fig. 4, to a thickness of 0.25

**Table 1 Comparison of properties for compacts produced from copper powders by cold gas-dynamic spraying**

| | Material | | | |
|---|---|---|---|---|
| | Direct reduction (SCM-500RL) | Gas-atomized (Acupowder 500) | Reference Material | Remarks |
| **Property** | | | | |
| Majority particle Diameter range ($\mu$m) | 10 – 20 | 9 – 25 | N/A | . . . |
| Spray conditions Pressure (MPa) | 2.0 – 2.4 | 2.0 – 2.4 | . . . | . . . |
| Gas temperature (°C) | 315 | 315 | . . . | . . . |
| Stand off distance (mm) | 25 | 25 | . . . | . . . |
| Nozzle dimensions (mm) | $2 \times 10$ | $2 \times 10$ | . . . | . . . |
| Oxygen content (wt.%) | . . . | . . . | 0.029 | C11100 ETP copper |
| Specified as loss on $H_2$ anneal | 0.20 | 0.25 | . . . | . . . |
| As-received powder (measured) | 0.77 | 0.29 | 0.10 | Starting powder[12] |
| Compact (measured) | 0.82 | 0.27 | 0.10 | Cold-spray copper compact[12] |
| Room temperature Young's modulus (GPa) | N/A | $108 \pm 9$ | 126 | (OFHC copper)[17] |
| | . . . | . . . | 25 – 37 | Vacuum plasma spray copper[18] |
| Microhardness (Knoop) | $140 \pm 10$ | $160 \pm 8$ | $64 \pm 7$ | C-11100 ETP copper |
| | . . . | . . . | 102 | Cold-spray copper-Vickers hardness[12] |
| | . . . | . . . | 81 | Copper reference-Vickers hardness[12] |
| | . . . | $52 \pm 6$ | . . . | Vacuum-annealed compact, 800 °C, 6 h |
| Maximum coating compressive stress (MPa) | 60 | 120 | . . . | . . . |
| Electrical resistivity | . . . | 2.4 | 1.7 | Pure copper[19] |
| ($\mu\Omega$– cm) | . . . | . . . | >10E + 11 | Cold-spray compact[20] |
| | . . . | . . . | 6 | Twin-wire arc spray[20] |
| | . . . | . . . | 5.45 | Plasma-arc spray[20] |

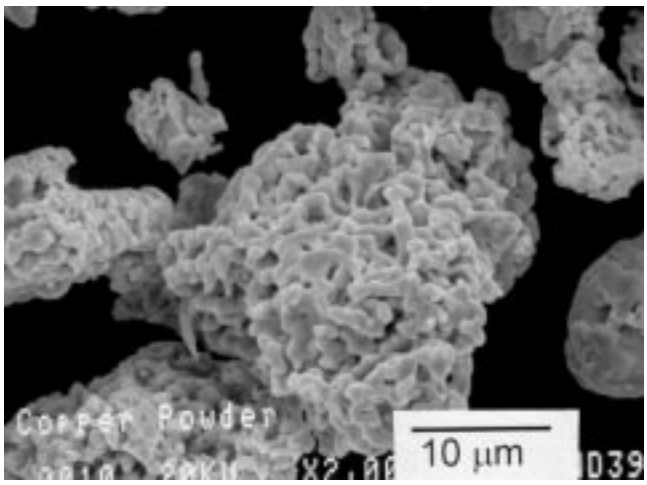


**Fig. 1** Scanning electron micrograph of as-received, direct-reduction copper powder

mm, punching 3 mm diameter discs and polishing with SiC abrasives of 600 and 1000 grit to a thickness of 75 $\mu$m. These discs were subsequently thinned by dimpling with a Gatan 656 precision dimple grinder and cubic boron nitride abrasive to a thickness of 20 $\mu$m, and then thinned to electron transparency using the Gatan PIPS at 4° tilt with argon ions at 5 keV, with final bombardment of 1.7 keV for 15 min. The SCM copper samples were generally brittle and were often broken during sample preparation. Samples were examined in a JEOL 2000FX transmission electron microscope/scanning transmission electron microscope (Japan Electron Optics Ltd., Tokyo) with a LINK (Oxford Instruments, Concord, MA) AN 10000 microanalysis system.

**Mechanical Properties.** The composite residual stress in the coating layers and substrate was determined using the modified layer removal technique developed by Greving *et al.*[15] For these determinations, the as-deposited layers were mechanically ground to produce a planar surface, free of any waviness associated with irregularities of the deposition and having a final thickness of approximately 2 mm. The residual stress distribution as a function of depth from the planarized outer surface was measured for four separate specimen pieces of approximately $2.5 \times 2.5$ cm taken from each of the two different cold-sprayed coupons. The precise effect of this mechanical working of the deposit layer on the composite residual stress measurement in this particular instance is unknown, although abrasive layer removal is believed to be detrimental to the accuracy of the technique.[1] A measurement of residual stress versus depth for the SCM-500 material using this method was previously reported in Ref 11, where a net compressive stress on the order of 33 MPa was observed in the coating layer. Measurement of Young's modulus of the Acupowder 500 compact was performed using the composite cantilever method of Rybicki *et al.*[16] While the calculation of residual stress by the layer removal method is dominated by the Young's modulus of the substrate, a measure of Young's modulus for the coating can give some indication of the mechanical integrity of the deposited layer compared to the bulk material. Microhardness measurements of the two types of deposits were determined for ten separate areas on the cross section of the deposit using a Knoop indenter at 100 g load in order to give an indication of the extent of cold work developed by the impact process relative to annealed or wrought copper references.

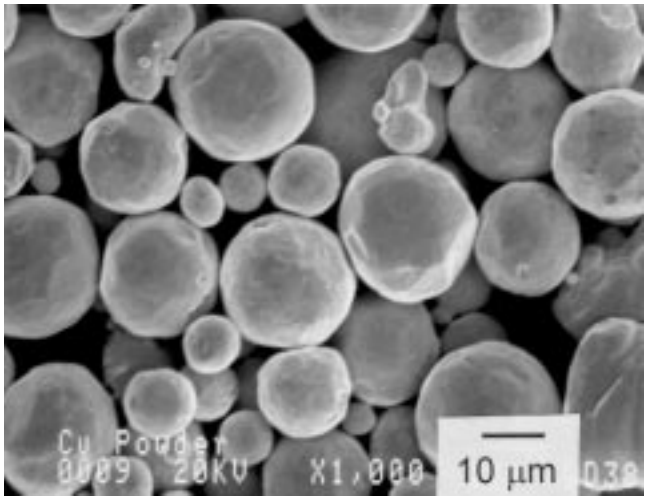


(**a**)

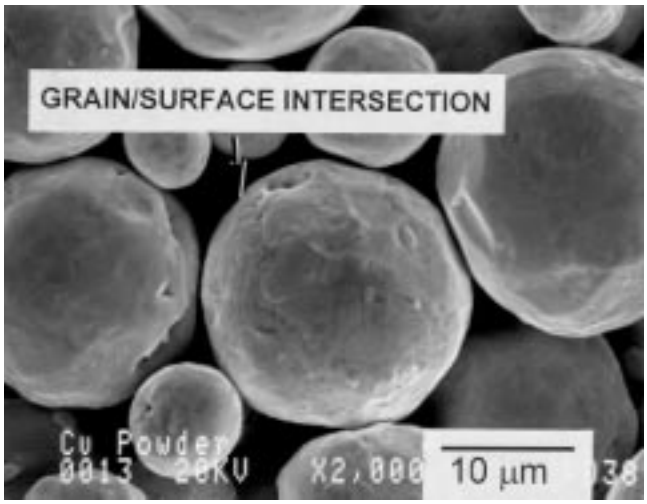


(**b**)

**Fig. 2** (**a**) Scanning electron micrograph of as-received, gas-atomized copper powder particles. (**b**) Higher magnification SEM photograph of gas-atomized copper particles showing surface grain intersections

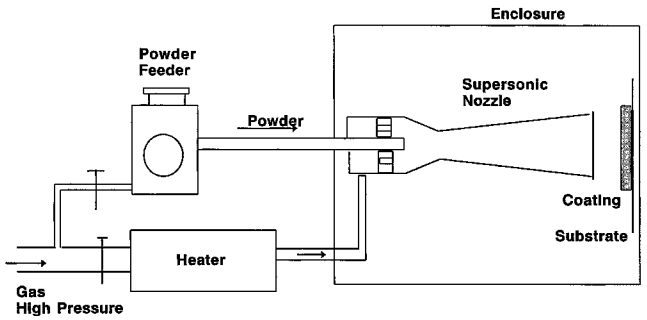


**Fig. 3** Schematic representation of the cold gas-dynamic spray process

**Electrical Resistivity.** The electrical resistivity of the cold-sprayed Acupowder 500 specimen was measured using a precision electrometer and current supply on a rectangular parallelepiped of material excised from the larger deposit by electrical discharge machining, and then polished metallographically

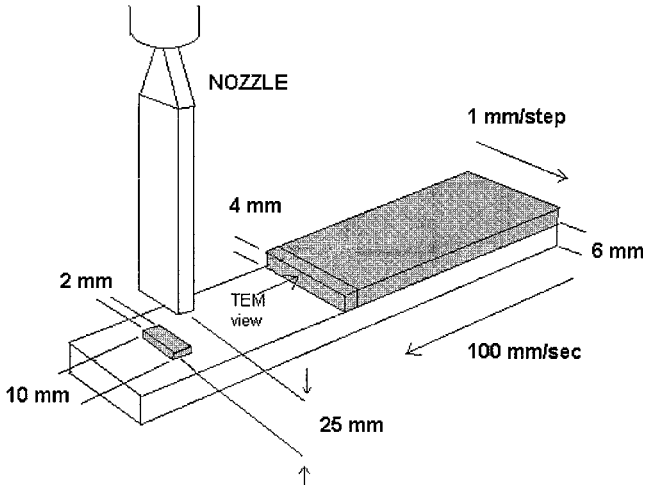


**Fig. 4** Sample and nozzle configuration for these experiment

to a smooth surface finish using 600 grit paper and alundum slurry. The specimen was approximately $2 \times 2 \times 30$ mm. There was not a sufficiently large sample of the SCM material for a comparative measurement.

**Annealing Studies.** Experiments to test the mobility of interparticle boundaries were conducted on small rods approximately $1 \times 1 \times 10$ mm, excised from the deposit layer by electrical discharge machining. A rod sample was placed in a miniature tube furnace and held under vacuum of at least $1.3 \times 10^{-3}$ Pa ($10^{-5}$ torr) at various temperatures ranging from approximately 650 to 850 °C and time periods of from 1 to 24 h. Cross-sectional pieces were then cut from the rod specimens for metallographic examination and comparison to the as-sprayed compact.

## 4. Results and Discussion

### 4.1 Microscopy

**Feedstock Powders.** The surface appearances of the as-received particles of the SCM-500 RL (direct reduction) and Acupowder 500 (gas atomized) feedstock powders are compared in the SEM photos of Fig. 1 and 2 (a and b), respectively. As expected, the powder particles produced by direct reduction show highly convoluted surfaces, while the gas-atomized particles are generally more spherical as may be expected, although discrete internal grain boundaries may be seen intersecting the surfaces of the particles. Fig. 5(a) shows an optical micrograph of the unetched cross-sectional structure of a particle of the direct-reduction material, illustrating the extent of internal porosity and voiding. Figure 5(b) shows a particle of this material seen by TEM showing both internal grain structure of the particle and a layer of surface oxidation with thickness on the order of 50 nm. The surface oxide layer on the direct-reduction particles was found to consist of discrete crystallites of $Cu_2O$, confirmed by electron diffraction. The higher oxygen content in the starting powder (Table 1) of the direct-reduction material is thus understandable in terms of the convoluted structure of the particles and observable oxide layer, as seen by TEM. The pre-existing oxide layers found on surfaces of the direct-reduction powder particles are ultimately incorporated into the compact produced by cold

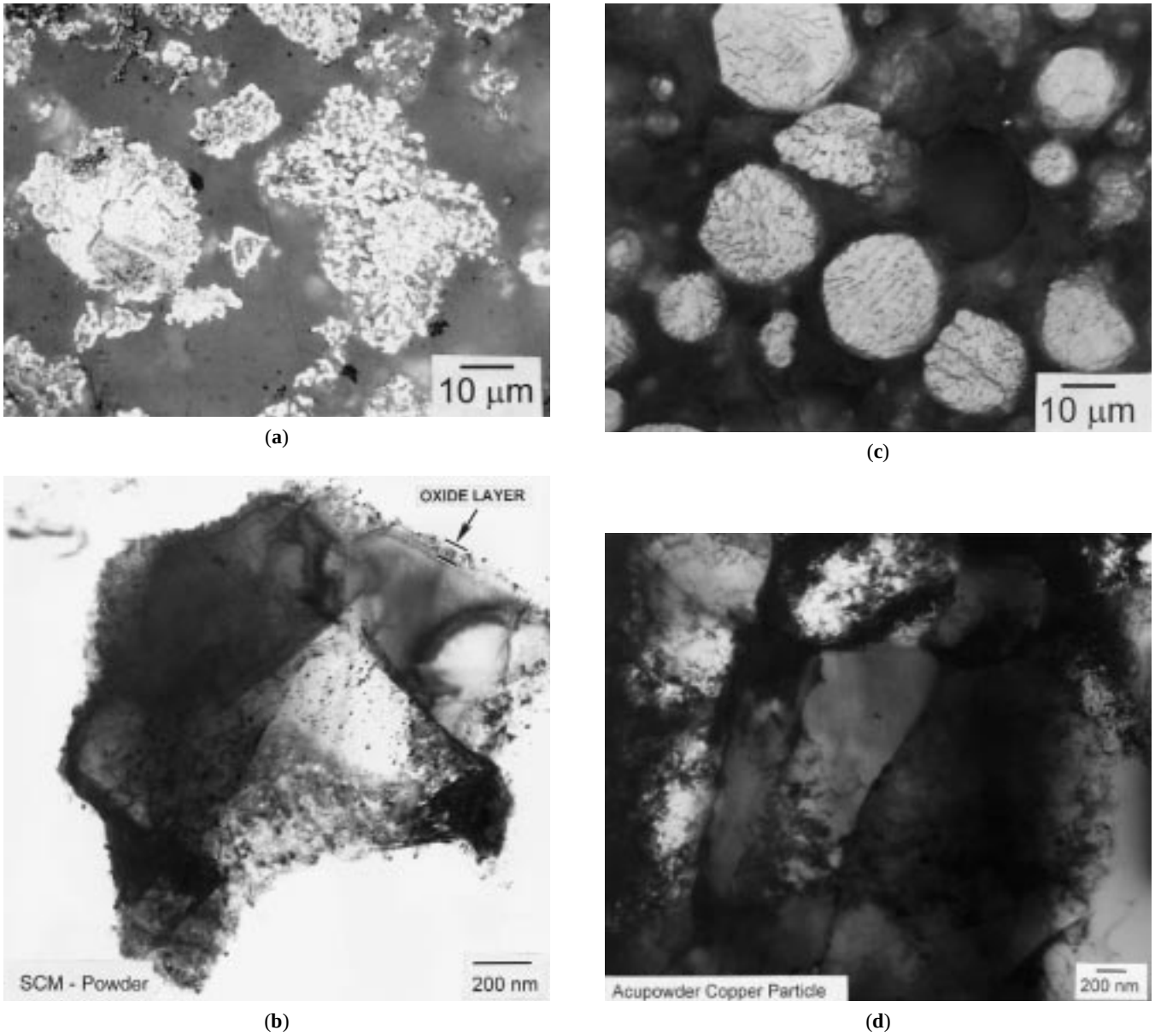


**Fig. 5** (**a**) Optical micrograph of polished cross section of direct-reduction copper particles showing internal structure. (**b**) Transmission electron micrograph of direct-reduction copper particle showing surface oxide layer. (**c**) Optical micrograph of polished and etched cross section of as-received, gas-atomized copper powder particles revealing internal grain structure. (**d**) Transmission electron micrograph of as-received, gas-atomized copper powder particle showing internal subgrain structure and intrinsic dislocation structure

spraying. In the optical micrograph of Fig. 5(c), the internal grain structure of the gas-atomized copper may be seen with visible grains on the order of several micrometers in dimension. A transmission electron micrograph of a particle of the gas-atomized powder is shown in Fig. 5(d), where subgrains with dimensions less than a micrometer are revealed, along with internal dislocation networks, presumed to be characteristic of the solidified powder. No detectable surface oxides were observed in the gas-atomized powder sample thinned for TEM. The general absence of discernible oxides in the gas-atomized powder is believed to permit development of compacts with little or no copper oxide film or particles at the interparticle boundaries.

**Deposit Layers.** A cross-sectional optical micrograph of the layer produced from the direct-reduction copper powder is shown in Fig. 6(a), where the plane of the section is perpendicular to the target coupon surface. At this magnification, the trapped oxide particles are not discernible. Transmission electron microscopy of the direct-reduction copper powder compact is typified by Fig. 7, where the extent of oxide particle retention can be seen in the form of rows of trapped oxide particles delineating former surfaces on the feedstock particles. Since the feedstock particles appeared to have relatively uniform oxide layers on their highly convoluted surfaces, the final deposit layer simply incorporated these surfaces, the interleaving bulk

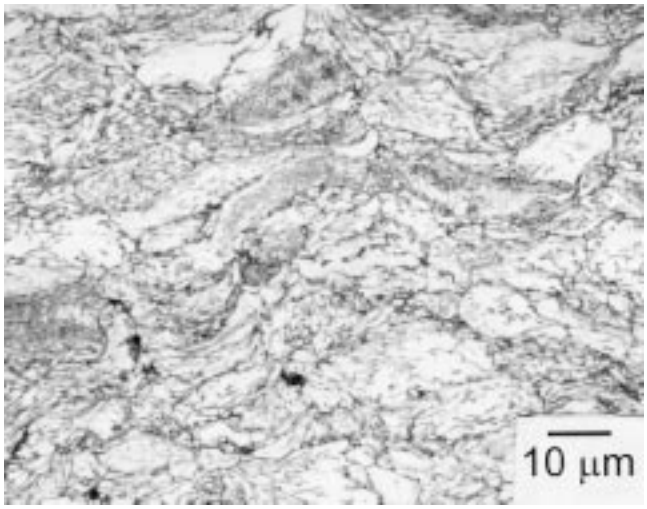


(**a**)

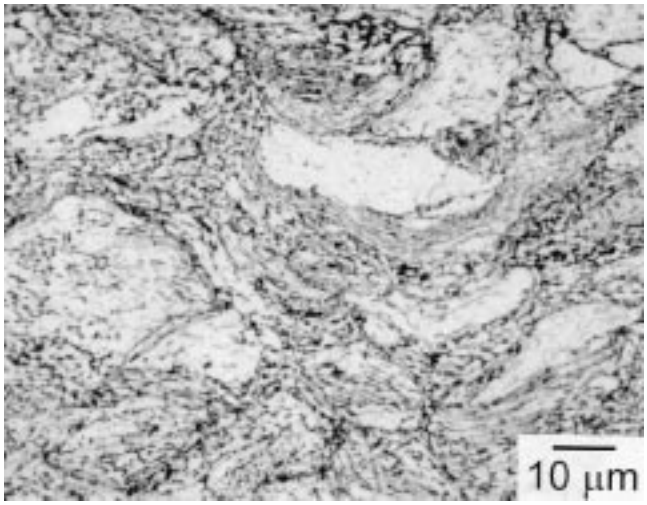


(**b**)

**Fig. 6** (**a**) Optical micrograph of a cross section of the cold-spray compact of direct-reduction copper powder cut perpendicular to the sprayed surface. (**b**) Micrograph of similar cross section following vacuum anneal for 6 h at 720 °C

material being flattened during the compaction process. Grain regions adjacent to the incorporated oxide particle arrays and strings appear to be recrystallized and relatively free of dislocation arrays. Fractographs of a specimen of the as-compacted, direct-reduction copper, shown in Fig. 8, suggest a pseudo grain structure defined by apparently fractured interparticle boundaries. The entrained oxide particle arrays, visible by TEM (Fig. 7), are not discernible on the fracture surface as observed by SEM. Particulate debris appearing on the fracture surfaces at higher magnification (Fig. 8(b)), however, is believed to be deformed copper from the smallest subparticles of the feedstock particle, delineated by thin (~50 nm) oxide skins, as were revealed by TEM.

An optical micrograph of the polished cross section of a deposit formed from the gas-atomized copper powder is shown in Fig. 9(a) and is generally indistinguishable at this magnification from that

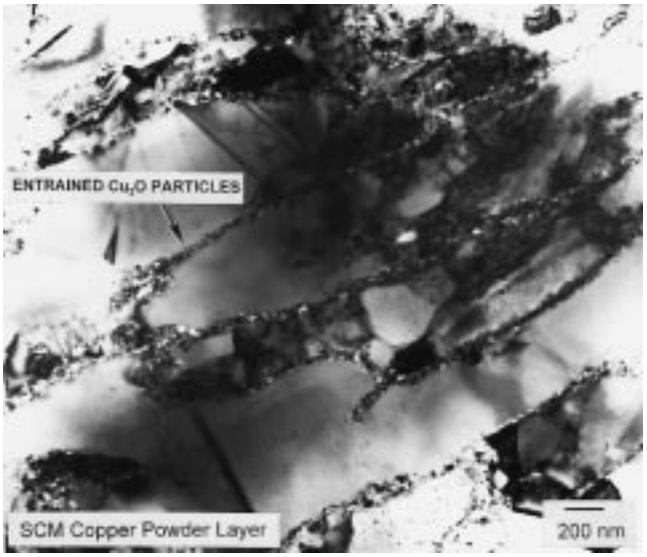


**Fig. 7** Transmission electron micrograph of a compact formed from direct-reduction copper particles exhibiting arrays of entrained copper oxide particulates at internal boundaries

formed from the direct-reduction copper powder. A transmission electron micrograph of the gas-atomized copper compact is shown in Fig. 10, where a linear array of voids, interpreted to be the remnant of an interparticle boundary, is marked. The subparticle structure of the layer shows a cellular structure, reminiscent of worked metals, wherein the smallest cellular regions are on the order of hundreds of nanometers in extent with relatively featureless interiors. The microstructure appears to be dense and generally free of discernible oxide particle inclusions. There was no immediate means for distinguishing interparticle boundaries in the layer other than to seek relatively linear features with discontinuous subgrains or strings of voids. The quality of these interparticle boundaries is critical since such interfaces may chemically "pin" recrystallization or grain growth, thus limiting post deposition annealing and microstructural refinements that may be required to improve electrical and thermal behavior of copper. This aspect is treated in the discussion of annealing studies.

### 4.2 Mechanical Properties

Table 1 summarizes mechanical property data for the compacted copper materials as determined by microhardness, Young's modulus, and through-coating residual stress distribution. Microhardness of both the direct-reduction copper compact and gas-atomized compact was greater than the reference material (C11100 ETP copper strip) by a factor of several times (*e.g.*, 140 to 160 versus 64 Knoop-HK). Other researchers[12] showed a compact hardness of 102 (Vickers- HV) versus 81 for the reference material. These results suggest that at least a portion of the cold work introduced during the spray process is retained in the coating. Room-temperature Young's modulus of the as-sprayed, gas-atomized copper compact was measured to be 108 ± 9 GPa in comparison to the handbook value of 126 GPa. Measurement of Young's modulus of vacuum plasma-deposited copper by Montavon *et al.*[18] showed a range of from 25 to 37 GPa, depending on the level of porosity in the material. Rybicki *et al.*[16]

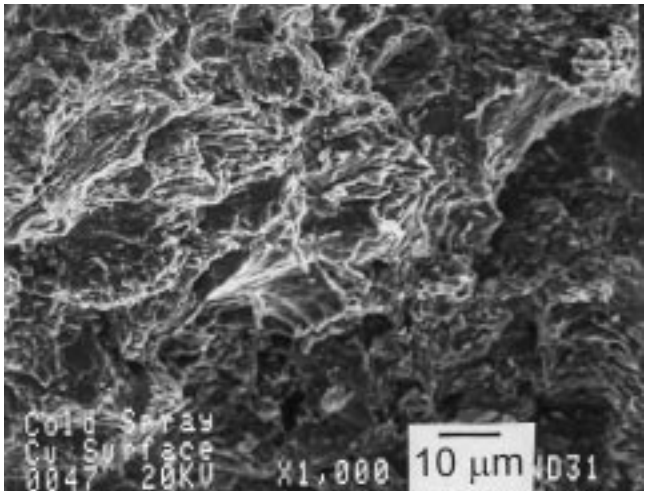


(**a**)

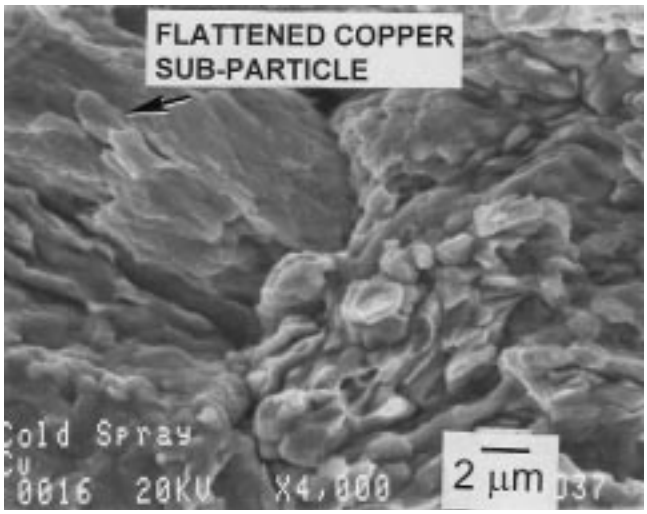


(**b**)

**Fig. 8** (**a**) SEM image of fracture surface of cold-spray compact produced from direct-reduction copper powder (**b**) Higher magnification image showing smallest isolated subregions of the starting particulate as flakes

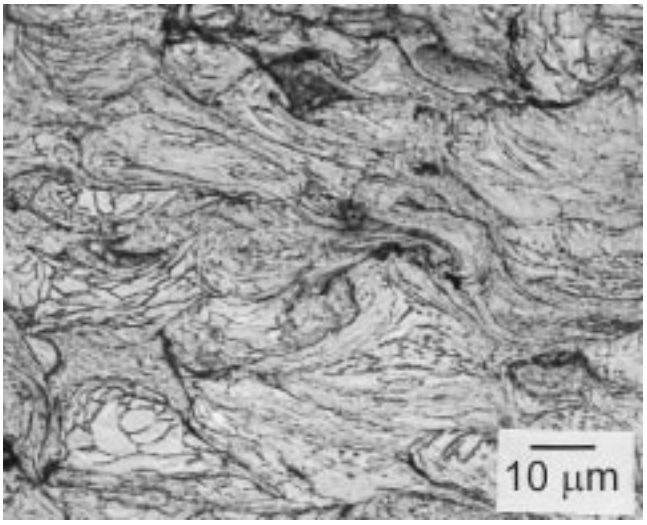


(**a**)

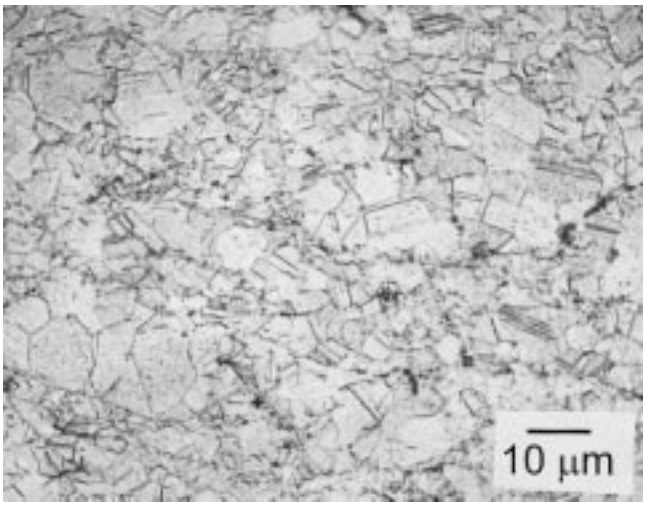


(**b**)

**Fig. 9** (**a**) Optical micrograph of a copper compact formed by cold gas-dynamic spray of gas-atomized Acupowder 500 copper powder. (**b**) Gas-atomized copper compact after annealing in vacuum at 650 °C for 24 h

reported significantly lower Young's moduli for conventional (*e.g.*, wire arc, plasma) thermal spray deposits for a variety of materials than their bulk counterparts. In this regard, cold gas-dynamic spraying of the gas-atomized copper powder produced surprisingly high values of Young's modulus of nearly 85% of the bulk value. Other cold-spray experiments[19] on deposition of low-carbon steel have shown Young's modulus values in the range of 82 to 88% of that reported for the bulk material using the same measurement technique.

The through-coating residual stress distributions for the two copper materials are compared in Fig. 11, where the data point indicates the average for the four coupons measured and the error bars indicate the estimated standard deviation. The deposit layer produced from direct-reduction copper showed a characteristic compressive region in the surface of the substrate, as is often associated with the grit blast preparation process, and net compressive stress in the coating at an average value of approximately 33 MPa extending through the majority of the layer thickness, with a maximum compressive stress of approximately 60 MPa near the substrate interface. In the case of the gas-atomized copper compact, the interfacial compressive region extended into the coating to a greater extent with a maximum compressive stress adjacent to the interface of approximately 120 MPa. The coating exhibited a near-neutral stress through its central portion, reaching tensile stresses in the range of 60 to 80 MPa near the outer surface. Residual stress measurements in a variety of thermal-spray coatings using the modified layer removal method[15] indicate a tendency for tensile residual stresses, particularly in coatings made by plasma- or wire-arc processes. Coatings produced by high velocity processes, such as detonation gun or HVOF, may result in residual compressive stresses in the deposited layers. In this regard, cold gas-dynamic spraying produces deposits with intrinsic stress state similar to those of other high velocity processes.

### 4.3 Electrical Resistivity

The room-temperature electrical resistivity of the gas-atomized copper powder deposit was measured to be approximately 2.4 $\mu\Omega$ cm. The handbook value for pure, oxygen-free copper is 1.7 $\mu\Omega$ cm.[18] In another experimental determination of resistivity for a copper compact formed by cold gas-dynamic spraying, Ohmann[20] measured a resistivity of $>10^5$ $\Omega$ cm for a coating made from a feedstock material containing 0.21% oxygen. More conventional thermal-spray processes (*e.g.*, plasma-arc and twin wire-arc) yielded resistivities of 5.45 and 6.35 $\mu\Omega$ cm, respectively. The present work indicates a more favorable outcome for the electrical resisitivity of the cold gas-dynamically sprayed copper than that measured by Ohmann, suggesting that starting materials and deposition conditions may be critically important for optimizing electrical conductivity. While the starting powder used for Ohman's specimens contained less residual oxygen than the powders used here, a micrograph of the final deposit indicated generally high porosity and a poor quality of the particle deformation, which is apparently needed to effect breakup of any surface oxide skins and develop metal/metal contact of the feedstock particles.

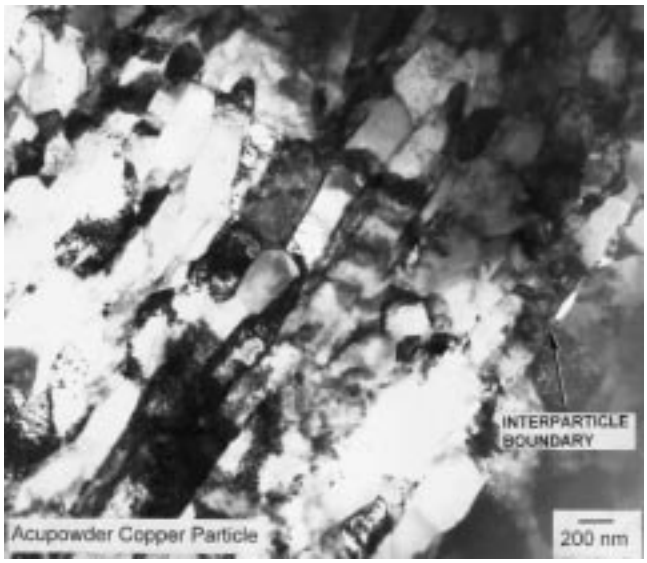


**Fig. 10** Transmission electron micrograph of copper compact formed by cold gas-dynamic spraying of gas-atomized copper powder

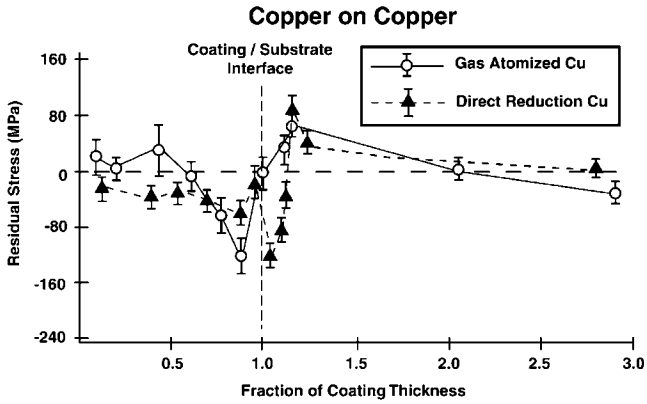


**Fig. 11** Comparison of through-thickness residual stress distributions measured by the modified layer-removal technique for compacts produced from gas atomized and direct-reduction copper powders

### 4.4 Annealing Studies

It was believed that the ability to thermally alter the microstructure of the as-sprayed copper deposits through processes of recrystallization and grain growth would effectively permit an assessment of the quality of the interparticle interfaces insofar as their role in either preventing or allowing grain-boundary migration during annealing of the as-sprayed deposits.

In the case of the direct-reduction copper compacts, oxide decoration of interparticle boundaries effectively limited the ability of the structure to adopt an equiaxed grain structure after annealing to a temperature as high as 720 °C for a period of 6 h. Fig. 6(b) illustrates the postanneal microstructure of the direct-reduction copper compact showing effectively a similar appearance to the as-sprayed microstructure. Examination of a polished cross section of this compact following vacuum annealing (Fig. 12) shows coalescence of the $Cu_2O$ phase into particulates of approximately 1 $\mu$m. Arrays of these copper oxide particles appear to effectively pin the grain structure, which evolves on annealing from the sprayed compact.

In contrast to the annealing behavior of the deposit formed from direct-reduction copper powder, the gas-atomized copper compact exhibited grain growth apparently uninhibited by oxide particles entrained in the as-sprayed structure. Fig. 9(a) and (b) compare the as-sprayed and annealed microstructures of the gas-atomized copper deposit following a 24 h vacuum anneal at 650 °C. Attempts to anneal at higher temperatures did appear to evoke increased porosity in the structure, although the mechanism is not understood. Similarly, an attempt to anneal the gas-atomized copper compact under hydrogen gas to assist in reduction of remnant oxides instead seemed to promote porosity and internal voiding, perhaps due to water formation or gas trapping.

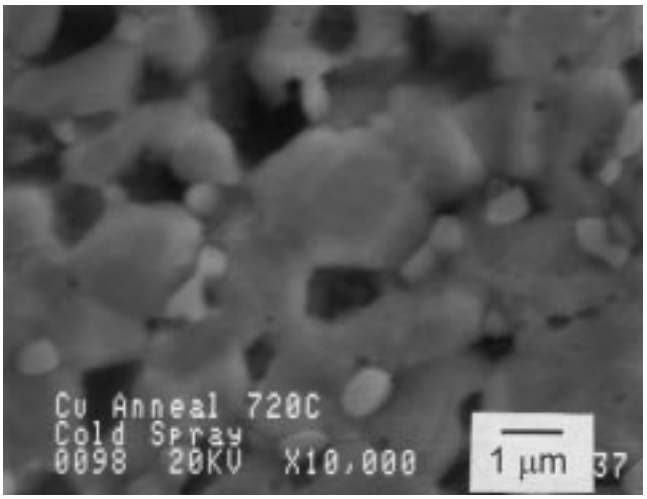


**Fig. 12** Scanning electron micrograph of a polished cross section of vacuum annealed direct-reduction copper-powder compact revealing coalesced $Cu_2O$ particles at copper grain boundaries

Annealing of the gas-atomized copper deposit for 8 h at 700 °C under vacuum resulted in a change in fracture mode as well as recrystallization and grain growth. Figure 13(a) illustrates a typical fracture of the as-sprayed, gas-atomized copper showing a "granular" appearance suggestive of fracture paths associated with the interparticle boundaries of the compact. Figure 13(b) shows a fracture surface of the compact after the 700 °C anneal, where the mode is now seen to be ductile, as evidenced by the void coalescence. Remnant particles (unidentified composition) may be seen in some of the void "pockets," as is typical of fracture in a ductile material with a dispersed harder phase. The annealing studies, while very rudimentary, show that the higher purity, gas-atomized copper powder compact can undergo some level of microstructural refinement and recrystallization, thereby relieving much of the internal disruption developed during the cold compaction process. The ability to conduct such secondary processes in cold-spray compacts may be useful in developing more complete materials processing schemes based on this technology.

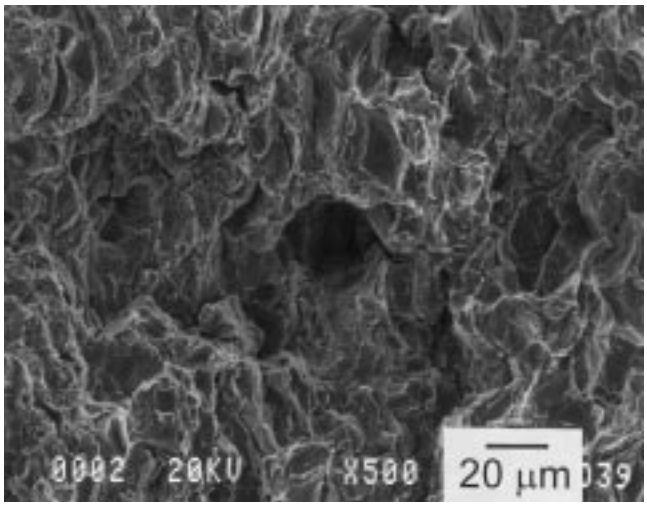


(**a**)

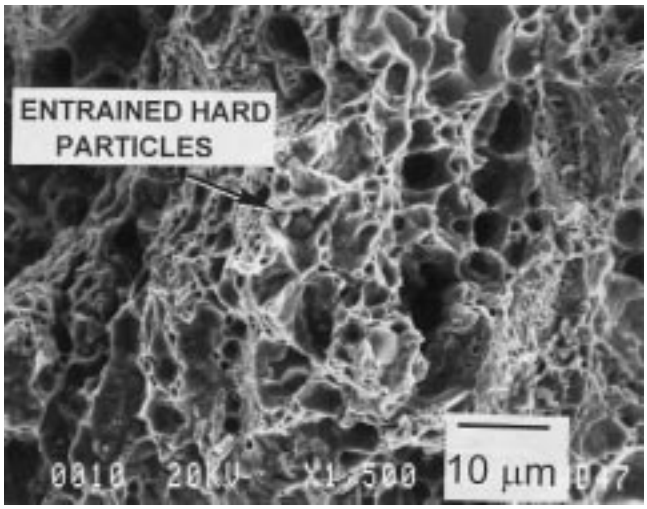


(**b**)

**Fig. 13** (**a**) Fracture surface of as-sprayed compact produced from gas-atomized copper powder. (**b**) Fracture surface of gas-atomized copper compact following anneal at 700 °C for 8 h

## 5. Summary

Copper deposit layers produced by the cold gas-dynamic spray method using two feedstock powders with different morphologies and oxide contents showed microstructures that reflected the quality of the starting materials, as might be expected in such a cold-compaction process. For example, surface oxide films formed on the highly convoluted surfaces of a direct-reduction copper powder become incorporated in the cold-sprayed compact. The prior surface oxides, now entrained as "interparticle" boundaries, thwart such refinement processes as grain growth. With a higher purity, gas-atomized copper feedstock powder, the sprayed deposit exhibited Young's modulus and electrical conductivity that were more bulklike than values reported in the literature for copper coatings produced using more traditional thermal-spray processes such as plasma- or wire-arc spraying, which involve liquefaction of the feedstock. The ability to anneal and refine the as-sprayed microstructure for a low-oxide, copper feedstock in these experiments suggests that such cold-spray deposition of other high-purity metals and composites may be only an initial step in developing coatings and free-standing structures of improved metallurgical and physical properties, in comparison to those achieved using more traditional thermal-spray processing.

### Acknowledgments

This work was conducted, in part, in conjunction with a consortium of companies under the sponsorship of the National Center for Manufacturing Sciences (NCMS, Ann Arbor, MI). The original participant companies included General Motors Corporation, General Electric - Aircraft Engines, Pratt and Whitney Division of United Technologies, Flame Spray Industries, and TubalCain Company. Dr. Anatolii Papyrin prepared the specimens used in this work under contract with NCMS. The authors thank Dr. Shaun McCarthy for measurement of electrical properties, Floyd Alberts for assistance in metallography, Ron Cooper for scanning electron microscopy, and Gerry Grab and Scott Badgley for assistance with vacuum annealing. We thank Drs. Edmund F. Rybicki, John R. Shadley, and Roy T. McGrann, University of Tulsa, for mechanical properties measurements. Dave Ohman, Thermal Spray Technologies, Inc., provided data in advance of the publication of his dissertation.

### References

1. T.W. Clyne and S.C. Gill: *J. Thermal Spray Technol.,* 1996, vol. 5, pp. 401-18.
2. Y.A. Kharlamov: *Mater. Sci. Eng.,* 1987, vol. 93, pp. 1-37.
3. G.H. Smith, R.C. Eschenbach, and J.F. Pelton: U.S. Patent 2,861,900, Nov. 25, 1958.
4. J.A. Browning: *J. Thermal Spray Technol.,* 1992, vol. 1, pp. 289-92.
5. C.F. Rocheville: U.S. Patent 3,100,724, Aug. 13, 1963.
6. A.P. Alkhimov, V.F. Kosarev, and A.N. Papyrin: *Sov. Phys. Dokl.,* 1990, vol. 35, pp. 1047-49.
7. A.P. Alkhimov, A.N. Papyrin, V.F. Kosarev, N.I. Nesterovich, and M.M. Shushpanov: U.S. Patent 5,302,414, Apr. 12, 1994.
8. H. Gabel and R. Tapphorn: *J. Met.,* 1997, vol. 49 (8), pp. 31-33.
9. R.B. Bhagat, M.F. Amateau, A. Papyrin, J.C. Conway, Jr., B. Stutzman, and B. Jones: *Thermal Spray: A United Forum for Scientific and Tech-*

*nological Advances*, ASM International, Materials Park, OH, 1998, pp. 361-67.
10. R.C. McCune, A.N. Papyrin, J.N. Hall, W.L. Riggs II, and P.H. Zajchowski: in *Advances in Thermal Spray Science and Technology*, C.C. Berndt and S. Sampath, eds., ASM International, Materials Park, OH, 1995, pp. 1-5.
11. R.C. McCune, W.T. Donlon, E.L. Cartwright, A.N. Papyrin, E.F. Rybicki, and J.R. Shadley: in *Thermal Spray: Practical Solutions for Engineering Problems*, C.C. Berndt, ed., ASM International, Materials Park, OH, 1996, pp. 397-403.
12. T.H. Vansteenkiste, J.R. Smith, R.E. Teets, J.J. Moleski, D.W. Gorkiewicz, R.P. Tison, D.R. Marantz, K.A. Kowalsky, W.L. Riggs II, P.H. Zajchowski, B. Pilsner, R.C. McCune, and K.J. Barnett: *Surf. Coatings Technol.*, 1999, vol. 111 (1), pp. 62-71.
13. R.C. Dykhuizen and M.F. Smith: *J. Thermal Spray Technol.*, 1998, vol. 7 (2), pp. 205-12.
14. D. Raybould: *J. Mater. Sci.*, 1981, vol. 16, pp. 589-98.
15. D.J. Greving, E.F. Rybicki, and J.R. Shadley: *J. Thermal Spray Technol.*, 1995, vol. 3, pp. 379-88.
16. E.F. Rybicki, J.R. Shadley, Y. Xiong, and D.J. Greving: *J. Thermal Spray Technol.*, 1995, vol. 4 (4), pp. 377-83.
17. *INCRA Monographs on the Metallurgy of Copper*, International Copper Association, Inc., New York, NY, 1992.
18. G. Montavon, B. Robert, C. Verdy, V. Monin, K.E. Atcholi, and C. Coddet: in *Thermal Spray: Practical Solutions for Engineering Problems*, C.C. Berndt, ed., ASM International, Materials Park, OH, 1996, pp. 827-32.
19. R.C. McCune, O.O. Popoola, W.T. Donlon, and E.L. Cartwright: *Rapid Prototyping and Manufacturing '98*, Society of Manufacturing Engineers, Dearborn, MI, 1998, pp. 495-520.
20. D. Ohmannn: Master's Thesis, University of Wisconsin, Madison, WI, 1998.